scientific reports

Check for updates

OPEN

Existence of edge modes in periodic microstrip transmission line

Aleksey Girich[1], Liubov Ivzhenko[2]✉, Ganna Kharchenko[1], Sergey Polevoy[1], Sergey Tarapov[1,3,4], Maciej Krawczyk[2] & Jarosław W. Kłos[2]

The microstrip of modulated width is a realization of a one-dimensional photonic crystal operating in the microwave regime. Like any photonic crystal, the periodic microstrip is characterised by the presence of frequency bands and band gaps that enable and prohibit wave propagation, respectively. The frequency bands for microstrip of the symmetric unit cell can be distinguished by 0 or π Zak phase. The sum of these topological parameters for all bands below a given frequency gap determines the value of the surface impedance at the end of the microstrip. We demonstrate that edge modes are absent in a finite microstrip terminated at both ends in the centres of unit cells, but they can be induced by adding the defected cells. Edge modes present at both ends of the microstrip enable microwave tunneling with high transitivity in the frequency gap with or without a change in phase. This has been demonstrated experimentally and developed in detail using numerical simulations and model calculations. The investigated system, with a doublet of edge modes in the frequency gap, can be considered as a narrow passband filter of high selectivity and characterised by a significant group delay.

The structures with periodic modulation of geometrical or material parameters in one dimension can be treated as artificial one-dimensional (1D) crystals. For such systems, one can address the fundamental question linking the topology of the band structure and the condition under which edge and interface states can be observed. The topological properties of the bands, such as a Zak phase[1,2], are used to indicate in which frequency gaps the edge states can be observed[3,4]. The experimental and theoretical studies of edge states in 1D artificial crystals have been carried out for photonic[5–12], phononic[13–15], plasmonic[16,17], magnonic[18] and electronic systems[19,20]. The microwave systems[21] in the form of periodic microstrips[22–26] , usually studied by electrical means, or the chains of cavities[17] also attract the attention of the researchers interested in the study of the bulk-edge correspondence.

The bulk parameters of a periodic microstrip consisting of two alternating sections of different widths determine the dispersion relation of electromagnetic waves. For truncated structures with given bulk properties, we can define the so-called surface impedance[4,27], which can be used to determine the conditions for the existence of edge (or interface) states at the microstrip ends (or at the junction of two microstrips). The surface impedance is strictly related to the Zak phase, and thus can be used to determine the necessary condition for the existence of the edge (interface) state[27,28]. These recent studies have focused on the interface states between two periodic microstrips, their topological properties and their potential applications. However, the edge microwave states localised at the edges of the periodic microstrip connected directly to input (or output) ports remain unexplored in terms of their topological properties and applications.

The most common application for microstrip of periodically modulated width is in the design of low-pass filters and stop-band filters, where a frequency gap above the first band is usually used[29–31]. The areas for new applications of these systems can be extended when we relate the existence of stop- and passbands sequences to the bandgap theory of wave excitations, well-known in photonics and solid state physics. One of such area is related to the topological properties of band structure and the existence of edge/interface states. While the existence of interface states is the result of an intentional proceeding (two periodic microstrips must be connected for them to appear), edge states can appear unintentionally (since each periodic microstrip is in fact a finite structure). Therefore, knowledge of the conditions for the existence of edge states allows them to be eliminated or deliberately exploited in certain applications.

[1]O. Ya. Usikov Institute for Radiophysics and Electronics NAS of Ukraine, Kharkiv, Ukraine. [2]ISQI, Faculty of Physics, Adam Mickiewicz University, Poznan, Poland. [3]Gebze Technical University, Gebze, Kocaeli, Turkey. [4]Karazin Kharkiv National University, Kharkiv, Ukraine. ✉email: ivzhenko@amu.edu.pl

In this work we study experimentally and numerically the edge states in finite microstrip of modulated width—see Fig. 1. We show that the microwave edge states cannot exist at the ends of a periodic microstrip composed of centrosymmetric unit cells and terminating in symmetry points. We prove that this is the result of the topological property of the band structure (Fig. 2), i.e. the Zak phases of successive bands, and their relation to the surface impedance at the symmetry point. To induce the edge states, it is necessary to modify the shape of the first and last cells of the microstrip. When such a modification is introduced, the surface impedance in the gap can be matched to the impedance of the feed ports, and the narrow transmission band at frequencies within the band gap can be measured (Fig. 3). Importantly, the edge states form symmetric and antisymmetric pairs, allowing microwave signals to be tunneled through the finite microstrip with 0 or π phase shift (Fig. 4). This property suggests that a microstip with a doublet of edge states be used as a highly selective passband filter with a high value of group delay in the passband.

The paper is structured as follows. In the next section, we present the structure under investigation and the methods used in our study. We then analyze the band structure as a function of the bulk parameters—in these studies, we determine the symmetry of the Bloch functions at the edges of the bands and the Zak phases for successive bands. Next, we show that the edge modes cannot exist for the microstrip terminated at the symmetry points and investigate how the modifications of the first and last cells of the microstrip induce the edge states and tune their frequencies. At the end of the paper, the short section Discussion summarizes the main results of the paper. Finally, the experimental and numerical methods are described.

System

The experimentally investigated system is a microwave transmission line in the form of a periodically width-modulated microstrip composed of seven unit cells, as shown in Fig. 1a. Each of (five) bulk cells (Fig. 1b) consists of the section of wider microstrip (width $w_1 = 4$ mm) of length $l = 10$ mm connected to the neighboring cells by narrower sections (width $w_2 = 1.12$ mm). The length of the bulk unit cell d is 16 mm. The system ends with (two) edge cells, which have different dimensions from the bulk cell (width w_0, length l_0 of the wider segment, the total length d_0, and the shift p_0 of the wider segment with respect to the center of the cell). The values w_0, l_0, d_0 and p_0 are set to 9 mm, 1.5 mm, 11.5 mm and 0 mm, respectively. For reference, we also studied the system without edge cells of modified sizes, i.e. composed of five cells of the same dimensions. The microstrip is deposited on the insulating substrate characterized by a dielectric constant of $\varepsilon = 2.2 + \mathrm{i}\,0.0012$ and a thickness of $u = 0.381$ mm. The bottom side of the substrate is metallized and serves as the ground plane. The microstrip and the ground plane are made of copper with a conductivity of $\sigma = 58$ MS/m and a thickness of 35 μm.

A vector network analyser was used to measure the transmission spectra of the microwaves in the frequency range 8 - 20 GHz (see the photo of the experimental setup in Fig. 1a). The input and output of the microstrip are connected to a vector network analyzer with standard $Z_0 = 50\,\Omega$ impedance ports to measure the S_{21} transmission spectrum. For the theoretical studies, full electromagnetic simulations were carried out using *CST Microwave Studio* with the same parameters as in the experimental studies. More details on the methodology used can be found in the Methods section.

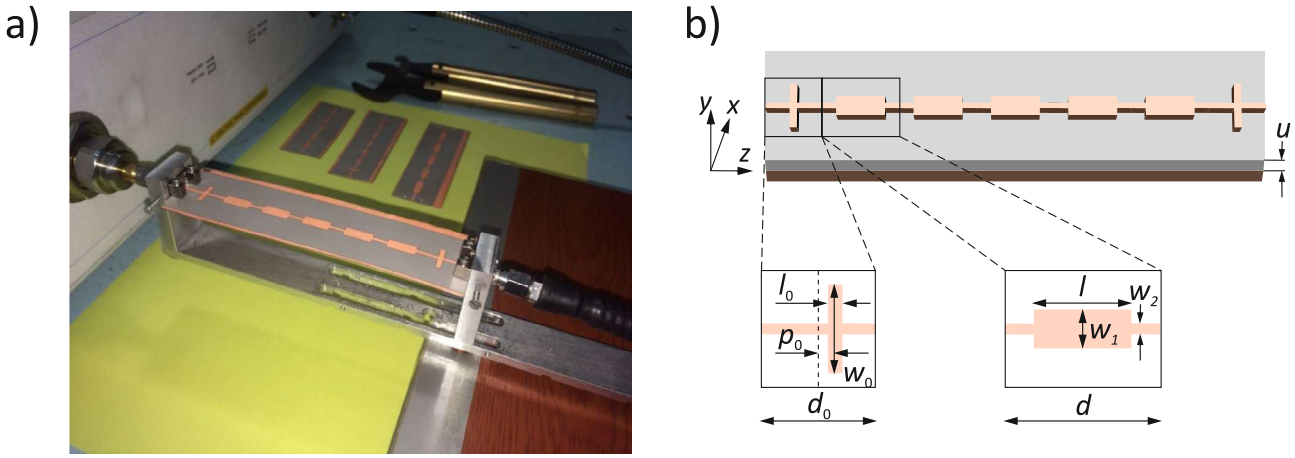

Figure 1. Periodic microstrip under investigation. (**a**) The photo of the experimental setup shows the microstrip connected to a vector network analyzer with standard $Z_0 = 50\ \Omega$ ports to measure the S_{21} spectrum. (**b**) The geometry of the system used in the numerical simulations. The microstrip, composed of five bulk cells and two edge cells, is placed on the substrate of thickness u with metallized bottom surface, which plays the role of the ground plane. The bulk and edge cells differ in size: d, and d_0, and in geometric parameters: (l,w), and (l_0, w_0), respectively. For the edge cell, we also considered the shift p_0 of the wider segment with respect to the center of the cell.

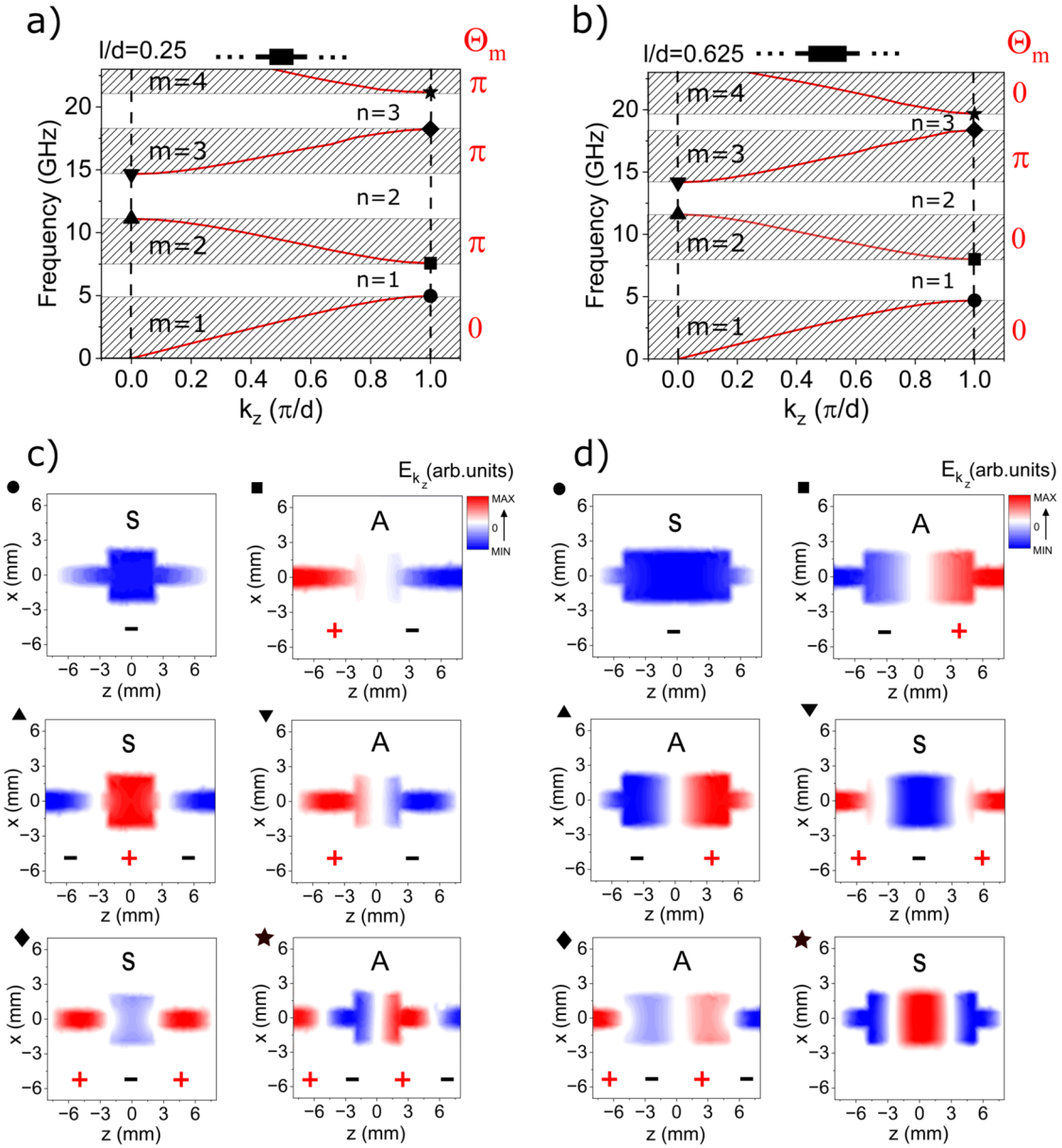

Figure 2. (**a**, **b**) The numerically calculated dispersion relation for an infinite periodic microstrip, for two selected values of the bulk parameter: (**a**) $l/d = 0.25$ and (**b**) $l/d = 0.625$. We have kept the period d constant and increased the length of the wider segment l by the cost of the length of the narrower segment $d - l$ (see the black schemes in the insets above (**a**) and (**b**)). The values 0 and π, printed in red on the right of sub-figures (GHz frequency range) and (**b**), denote the Zak phase θ_m for successive bands $m = 1, 2, 3, 4$. (**c**, **d**) Spatial distribution of the electric field amplitude of the Bloch functions $E_{m,k_z}(x, z)$, for (**c**) $l/d = 0.25$ and (**d**) $l/d = 0.625$. The intensity of the color indicates the amplitude, while the red and blue colors indicate opposite phases. It can be seen that the symmetry of the Bloch functions at the edges of the second (up-triangle, down-triangle) and third (diamond and star) gaps are switched between symmetric (S) and anti-symmetric (A), while we change l/d from (**c**) 0.25 to (**d**) 0.625. The systems for $d/l = 0.25$ and 0.625 are not topologically equivalent because they differ in Zak phases θ_m for corresponding bands.

Results

Measurements

The transmission spectrum for the system, which consists of five identical unit cells, is presented with the red line in Fig. 3c, while the transmission spectrum for the microstrip with edge cells of modified sizes is shown in Fig. 3d also with the red line. The results presents the transmission $|S_{21}(f)|$ in the range of 8–18 GHz. For the microstrip with undisturbed ends, a significant decline of the $|S_{21}|$ parameter is noted up to − 30 dB within the 11.5–15.0 GHz frequency range (Fig. 3c). The spectrum for the microstrip with modified edge cells is significantly different. In the range 11.5–15.0 GHz, there is a peak at 13.5 GHz of relatively high $|S_{21}| = -10$ dB, transmission.

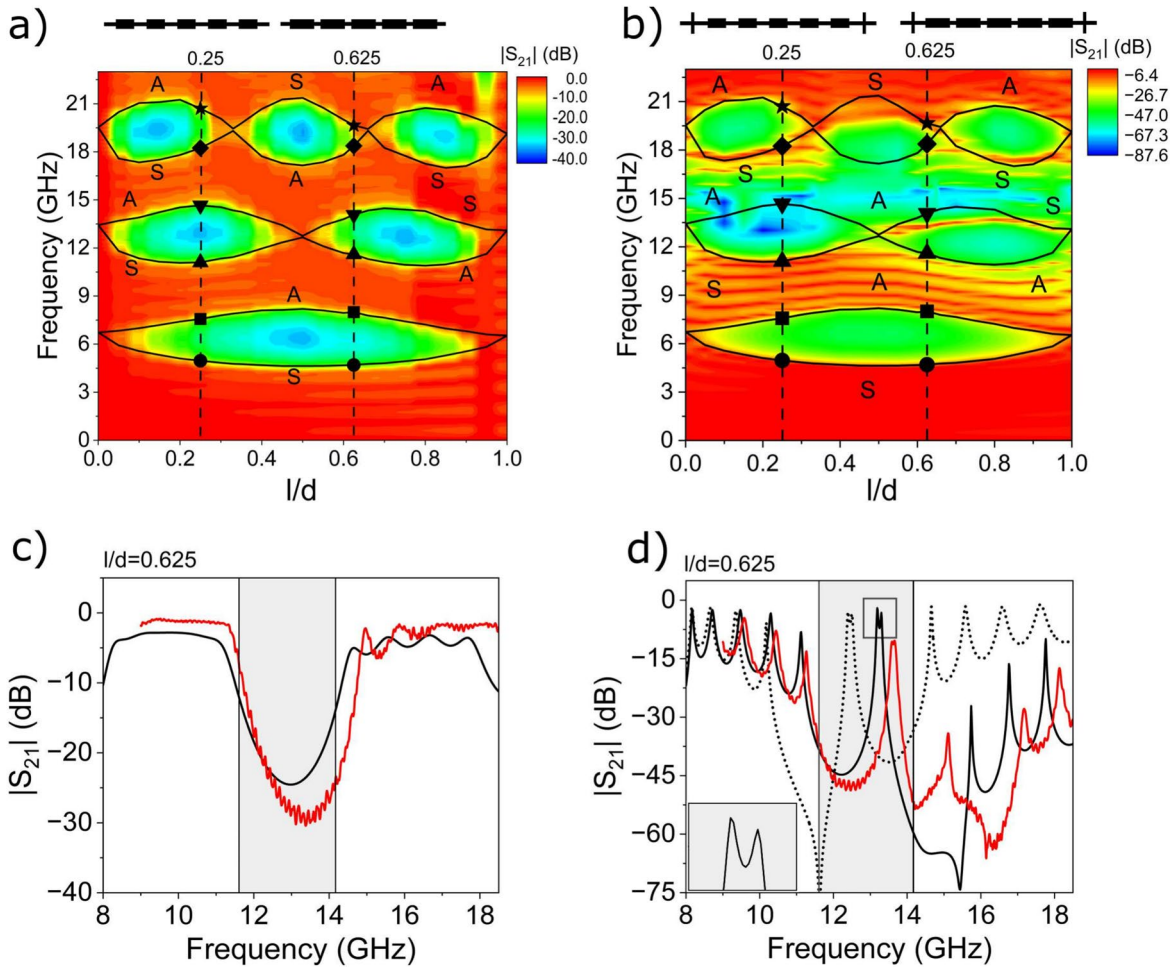

Figure 3. (**a**, **b**) The 2D transmission spectra of the finite periodic microstrip numerically calculated for different values of the bulk parameter: l/d. The solid black lines mark the edges of the bands for the semi-infinite microstrip, corresponding to $k_z = 0$ or $k_z = \pi/d$. Two ratios $l/d = 0.25$ and 0.625, for which the exemplary dispersion relations and Bloch functions were plotted in Fig. 2, are indicated by vertical dashed lines. The symmetry of the Bloch function at the edges of the band is indicated by the letters S and A. We considered the system (**a**) composed of five centrosymmetric cells and (**b**) its modification, where we added cells of modified sizes at the beginning and end of the microstrip—see the black schemes above (**a**) and (**b**). The sizes of the edge cells and all other parameters are the same as those given in the System section. (**c**, **d**) The cross-section of the 2D spectra (**a**, **b**) at $l/d = 0.625$ (solid black curves) is supplemented by the measured (red curve) transmission spectra for fabricated structures. For the microstrip with additional cells of modified sizes, we can identify the doublet transmission peaks (see enlarged view in the inset) in the second frequency gap (gray area), see their profiles in Fig. 4. The black dotted line in (**d**) shows the transmission spectra for the microstrip with modified edge cells: $d_0 = 12.5$ mm, $l_0 = 0.5$ mm, $w_0 = 11$ mm.

Additionally, the transmission for frequencies larger than 15 GHz is significantly attenuated, and the oscillatory character of $|S_{21}|$ is observed at frequencies both higher than 11.5 GHz and lower than 15 GHz.

Clearly, these spectral changes result from the addition of the edge cells of modified sizes. In the upcoming sections, we will demonstrate with numerical simulations and model calculations that the suppressed transmission between 11.5 and 15.0 GHz is due to the band gap introduced by the microstrip's periodicity, whereas the transmission peak about 13.5 GHz results from the microstrip's edge modes. In addition, we will argue that these edge modes result from the topological characteristics of the bands in an unmodified periodic microstrip, but necessarily supplemented with modified edge cells.

Band structure and topological properties of infinite system

The exemplary dispersions $f(k_z)$ (frequency f *versus* wave number k_z), computed numerically (for infinite periodic microstrip for two selected values of the relative length of the wider segment: $l/d = 0.25$ and 0.625, where the cell size is fixed at $d = 16$ mm), are plotted in Fig. 2a,b. The value of $l/d = 0.625$ and the values of other parameters (for both plotted dispersions) are the same as for the experimentally studied system. Both dispersions appear similar with the frequency bands (shaded areas, which are indexed by integer number m) separated by band gaps (white areas, indexed with n). It is worth noting that for frequencies higher than 24 GHz the dispersion

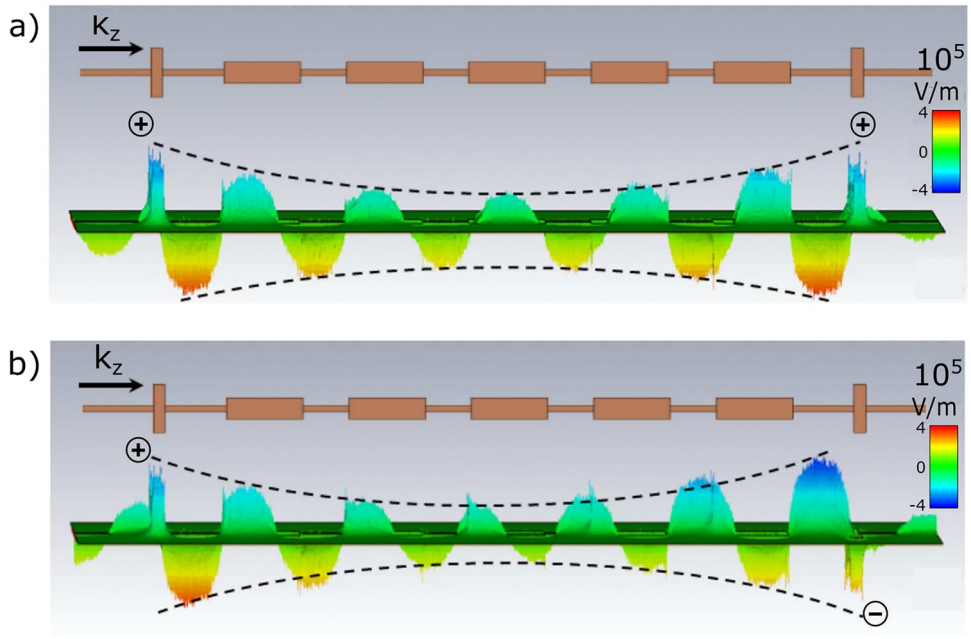

Figure 4. The calculated profiles of the edge modes (y-component of the electric field) observed in the second gap at the frequency 13.1 GHz for the microstrip with additional cells of modified geometry (see Fig. 3b,d)—we took the parameters corresponding to the experimentally realized structure. The pair of modes of very close frequencies shows the hyperbolic decay of the amplitude, when we move away from the edges of the microstrip. The modes form a double peak in the transmission spectrum—see Fig. 3d. The slight frequency splitting of this doublet results from the overlapping of the exponentially decaying 'tails' of the modes in the center for the structure, which is different for the mode that (**a**) does not flip and (**b**) does flip its phase (see '+' and '−' signs) as the electromagnetic wave tunnels between the edges.

relation is more complicated, as it contains branches representing, for example, the modes with nodal lines parallel to the waveguide axis. In our work, we will limit ourselves only to the bands of the lowest frequencies, where modes are quantized only along the microstrip axis (as in Fig. 2). For the microstrip with a dielectric spacer placed only between the signal line and the ground plane, we are dealing with hybrid TM-TE modes[29]. However, the considered microstrip is electrically very thin—the thickness of the spacer u is much smaller than the wavelength of the propagating field: $u \ll \lambda$. For such a system, the fields are quasi-TEM and there is no need to distinguish between TM and TE modes. To present the spatial profiles of the modes, we have shown the out-of-plane (i.e. the y—component) of the electric field.

It can be seen on the maps plotted in Fig. 2c,d, which show the profiles of the y-component of the electric field in a single unit cell for the frequencies from the edges of the bands/gaps (we assume the electric (magnetic) field is polarized in y- (x-) direction). The profiles are symmetric S or antisymmetric A while reversed in the z-direction. However, the symmetries of modes of some bands are different for $l/d = 0.25$ and $l/d = 0.625$. In particular, at the bottom (top) of the second gap—$n = 2$, the profiles of the Bloch functions are symmetric (antisymmetric) for $l/d = 0.25$ and antisymmetric (symmetric) for $l/d = 0.625$. This means that if we continuously change the ratio l/d between the values 0.25 and 0.625, at some value the exchange in the mode symmetry between the bands surrounding the second gap will occur. We will see that these changes are related to the closing and reopening of the gap(s) at certain values of the ratio l/d and connected with the changes of the bands' Zak phases θ_m.

This effect is illustrated in Fig. 3a showing numerically calculated transmission spectra $|S_{21}|$ in dependence on l/d. Here, the black lines mark the edges of the bands/gaps. We can see that throughout the l/d range ($0 < l/d < 1$), the first gap remains open, the second gap is closed once, the third gap is closed twice, and so on. It is clear that once we pass from $l/d = 0.25$ (Fig. 2a) to $l/d = 0.625$ (Fig. 2b), the order of the edges for the second and the third gap is reversed. The topological properties of the bands associated with such a change in the spectrum of a 1D photonic crystal can be described by the Zak phase θ_m[2,11,32] defined for each m^{th} band:

$$\theta_m = i \int_{-\pi/d}^{\pi/d} \left(\int_{\text{unit cell}} \varepsilon(z) u^*_{m,k_z}(z) \partial_{k_z} u_{m,k_z}(z) dz \right) dk_z, \tag{1}$$

where $\varepsilon(z)$ is the effective dielectric constant taking (when z is changing) two different values in wider and narrower section of microstrip (see Supplementary Information S1), and $u_{m,k_z}(z)$ is the periodic component of the Bloch function of the electric field $E_{m,k_z}(z) = u_{m,k_z}(z)e^{ik_z z}$, $[u_{m,k_z}(z) = u_{m,k_z}(z + d)]$. The Zak phase is equal to 0 or π for the system with centrosymmetric unit cell[2] and can be determined by the symmetry of the Bloch function $E_{m,k_z}(z)$[4,28,33,34]. If the Bloch function has the same symmetry on both edges of the band (i.e. the Bloch

function is symmetric (S) or antisymmetric (A) on both edges), then the Zak phase is equal to 0, otherwise, it is π. Therefore, the crossing of the edges of a given gap and the associated exchange of the gap boundaries observed during the continuous change of the bulk parameter l/d leads to the exchange of the Zak phase $0 \leftrightarrow \pi$.

We observe such crossings during the transition from $d/l = 0.25$ to $d/l = 0.625$ in Fig. 3a. For $l/d \approx 0.5$ ($l/d \approx 0.3$), the edges of the second (the third) gap are crossed. Therefore, the Zak phase is flipped once (at $l/d \approx 0.5$), from π to 0, for the second band, and twice, from π to 0 (at $l/d \approx 0.3$) and from 0 to π again (at $l/d \approx 0.7$), for the third band. As a result, the phase is the same (opposite) for the second (the third) band at $l/d = 0.25$ and 0.625 [see Fig. 2a,b and Eq. 5].

Bulk-edge correspondence

The spatially dependent wave impedance in an infinite periodic structure is called the Bloch impedance[29,35]:

$$Z_B(z,f) = \frac{E_{k_z}(z,f)}{H_{k_z}(z,f)}, \tag{2}$$

where $E_{k_z}(z)$ and $H_{k_z}(z)$ are the Bloch waves representing the electric and magnetic fields, and k_z is the frequency-dependent wave number, which takes real and complex values in the frequency bands and gaps, respectively. (We have omitted the band index m because Z_B is defined both in the frequency bands and in the frequency gaps).

Moving on to the finite microstrip, we need to consider the problem of impedance matching between the periodic microstrip and the ports. Let's consider the impedance at the input of finite microstrip ($z = -Nd$) composed of N cells and attached at the opposite end ($z = 0$) to the output port of the impedance Z_0:

$$Z_{\text{in}}(f) = Z_B(f)\frac{Z_0 + iZ_B(f)\tan(k_z Nd)}{Z_B(f) + iZ_0\tan(k_z Nd)}. \tag{3}$$

Equation 3 have a very similar form to the input impedance of loaded uniform transmission line[29]. Such similarity results from the Bloch theorem: $E_{k_z}(z+d) = E_{k_z}(z)$ and related periodicity of Bloch impedance: $Z_B(z+d,f) = Z_B(z,f)$, $Z_B(f)$ in (3) denotes Bloch impedance at the edges of unit cells. It is easy to notice that when the Bloch impedance is matched to the output port $Z_B(f) = Z_0$ then $Z_{\text{in}} = Z_0$. Consequently, the generator (input port) must be equal to the impedance of the load (output port) in order to ensure the complete impedance matching for the microstrip, which is composed of a sequence of identical unit cells. If the microstrip is terminated at the edge of the centrosymmetric unit cell, then the Bloch impedance at this termination is purely imaginary for the frequencies from the band gaps, and can be written as:

$$Z_B(f) = i\xi(f). \tag{4}$$

The function $\xi(f)$ changes monotonically as the frequency f rises from the bottom to the top of the frequency gap, where it reaches zero or pole[34]. The sign of $\xi(f)$ is then constant within a given n^{th} gap ($n = 1, 2, \ldots$), and moreover it can be determined by the Zak phases θ_m of all bands below it, i.e. for $m = 1, \ldots, n$:

$$\text{sign}(\xi_{\text{n}}) = (-1)^{\text{n}} \exp\left(\text{i}\sum_{\text{m}=1}^{\text{n}} \theta_{\text{m}}\right). \tag{5}$$

The formulas (5) and (4) express the bulk-edge correspondence because they relate the topological parameter of the bands (i.e., the Zak phase) to the parameter characteristic of the edge (i.e., the surface impedance) (see details in Supplementary Information S2). In the frequency gaps, the Bloch impedance Z_B taken at the edge of the centrosymmetric unit cell is imaginary (see Eq. 4). It is clear that a semi-infinite periodic microstrip cannot be matched at its symmetry point to the port (or semi-infinite but uniform microstrip) of real impedance Z_0, for any frequency in the range of any frequency gaps. Thus, the edge states cannot appear in the semi-infinite microstrip terminated at this point. For the sake of completeness, we still need to discuss the case of a finite microstrip and investigate whether an impedance mismatch at one end (e.g. to the output port) implies an inability to match the impedances at the opposite end (i.e. to the input port). To investigate this, the impedance of the loaded microstrip, as seen from its opposite end Z_{in}, must be calculated using (3) for the frequency gap, where: $k_z = n\frac{\pi}{d} + ik_I$ and $Z_B = i\xi$ (where both k_I and ξ are real). It can be shown that Z_{in} will be complex. That is, its imaginary part will be different from zero within each frequency gap: $\Im(Z_{\text{in}}) = (Z_0^2 + \xi^2)\tanh(k_I Nd)/(Z_0^2\tanh^2(k_I Nd) - \xi^2)$—please note that k_I has no zeros nor poles inside the gap.

This means that *the edge states in a microstrip composed of identical centrosymmetric unit cells could not exist*, independent of the topology of band structure, defined by the values of Zak phase (5)[34,36]. *To induce the edge state, we need to modify the geometry of the periodic microstrip near its termination*, which will result in a change in its impedance at band gap frequencies. Note that the problem of the mismatch between the imaginary value of the Bloch impedance and the real value of the port impedance Z_0 is similar to the case of the photonic crystal[6], where the impedance of the vacuum (or positive epsilon medium) is also real.

The color map in Fig. 3a shows the transmission spectrum $|S_{21}(f)|$ calculated for the periodic microstrip of finite length, depending on the bulk parameter l/d. The microstrip consists of five identical and symmetric cells connected to the 50 Ω ports. Therefore, the structure is terminated (i.e., the input and output ports are located) in the center of the narrower section of the unit cell. It is clear that in the frequency gaps calculated for infinite structure (delimited in Fig. 3a by black lines) the transmission is reduced and we do not observe any peaks (lines) indicating the presence of edge modes. In the next subsection, we will study the microstrip with additional cells placed at the end and beginning of the structure, which have different sizes from the bulk cells. We will show

that in such a system, we can find the edge modes. In addition, we will demonstrate the possibility of microwave tunneling that is mediated by the edge modes.

Edge modes

Figure 3b shows the transmission spectrum $|S_{21}(f)|$ in dependence on l/d calculated for the finite structure with additional edge cells (shown in Fig. 1b) located at the beginning and end of the periodic microstrip. The parameters describing the sizes of the first and last cells take the values $w_0 = 9$ mm, $l_0 = 1.5$ mm, $d_0 = 11.5$ mm, and $p_0 = 0$ (the same as for the experimentally realized system). The transmission spectrum preserves the main properties of the spectrum for the unperturbed microstrip shown in Fig. 3a. However, there are also differences: suppressing of $|S_{21}|$ in the 3rd band, and the presence of the additional line of enhanced transmission in the second gap opened for $l/d > 0.5$. It enters the gap from its top edge (for l/d close to 0.5) and crosses this edge again at $l/d \approx 0.9$.

To gain deeper insight into obtained numerical results, we plotted (in Fig. 3c,d) the calculated frequency-dependent transmission spectra (black solid lines) around the frequencies of the second band gap for the microstrip composed of five identical unit cells (Fig. 3c) and this microstrip with additional edge cells (Fig. 3d) for $d/l = 0.65$ (vertical dashed line in Fig. 3a,b, i.e., the same as in experimentally realized structures. There is a visible gap in the unperturbed microstrip (shown as a gray area in Fig. 3c), and two peaks of high transmission are observed within the gap around 13.27 GHz (for numerical results—black line) when edge cells are added to the microstrip, Fig. 3d. It is worth noting that the peak appears in the form of an almost degenerate doublet as is emphasized in the inset (with the values of the lower and higher frequency at 13.23 GHz and 13.33 GHz, respectively. We can identify these states as the edge modes that have a symmetric or antisymmetric profile, with respect to the center of the whole microstrip as shown in Fig. 4. This means that the phase of the resonantly tunneling microwaves is preserved or reversed, depending on how precisely we choose its frequency to activate one of the edge states.

These numerical results are superimposed with the results of measurements described in Sec. Measurements in Fig. 3c–d. The simulations successfully replicate the majority of the features in the measured transmission spectra. However, there is a slight shift of both the frequency gap and the position of the edge states within the gap by 0.5 GHz. This difference can be attributed to the parameter values assumed in simulations, which may slightly differ from their nominal values in the actual sample. In both spectra, numerical and measured, in Fig. 3d, we can see the deep anti-resonance, at 15.5 GHz (for simulations) or at 16.5 GHz (for the experiment). This anti-resonance significantly degrades the transmission through the third band. This unwanted effect is absent in the structure composed of identical cells. This means that the anti-resonance is induced by the presence of additional cells with modified sizes. The additional cells have a wide ($w_0 >> w$) and a short ($l_0 << l$) central section, which actually forms a pair of stubs. It is well known that, due to wave interference, the stub exhibits a sequence of resonances and anti-resonances in the transmission spectra[29], accompanied by significant changes in impedance, alternately switching between capacitive and inductive character. In our case, the cells with stubs ensure the impedance matching for the edge modes in the second frequency gap, but it is achieved at the expense of the anti-resonance in the third frequency band—see Supplementary Information S4 for more information.

As shown in the previous section, the second gap is topologically distinguishable in two ranges $l/d < 0.50$ and $l/d > 0.50$, separated by the point where its boundaries cross. For these two ranges, the sum of the Zak phases (for the bands below the second gap) is different (i.e. is equal to π for $l/d < 0.50$ and 0 for $l/d > 0.50$) and the corresponding signs of the imaginary component of Bloch impedance are opposite. We know that no edge states are observed in any gap, regardless of their topology, in the absence of additional reshaped cells at the beginning and the end of the microstrip. However, we have seen that the addition of such cells of specific geometry has a different effect on the appearance of edge states for the gaps differing in the sign of ξ_n. We are dealing with such a situation for the second frequency gap, where for $l/d > 0.50$ the doublet of edge states is visible in Fig. 3b and d. It shows that the changes in the topology of the band structure affect the Bloch impedance and strongly modify the conditions for the impedance match in the gap, and then significantly influence the conditions for the existence of edge modes. Similarly, we can interpret the states emerging near the edges of the third gap (Fig. 3b). One can notice lines inside the gap close to its top edge (around 20 GHz) for $l/d > 0.3$ and $l/d < 0.65$.

The geometrical parameters of the edge cells also affect the frequencies of the edge modes, which can be clearly seen in Fig. 3d, where for modified values of the parameters d_0 (increased by 1 mm), l_0 (increased by 1 mm), w_0 (decreased by 2 mm) the frequencies of the edge modes were shifted by 1 GHz (black dotted line). In order to study this problem systematically, we examined the effect of the parameters: w_0, l_0, d_0 on the transmission spectrum. In addition, we studied the role of the shift of the wider segment of the edge cell with respect to its center, i.e. we changed the parameter p_0. Fig. 5 shows the calculated transmission spectra for the finite microstrip where the chain of five identical bulk cells is supplemented by edge cells of modified sizes. We kept the sizes of the bulk cells the same as in the experiment ($d = 16$ mm, $l = 10$ mm, $w_1 = 4$ mm, $w_2 = 1.12$ mm) and changed only one of the geometrical parameters of the edge cell (all other parameters of the edge cell were the same as in the experimentally realized system: $l_0 = 1.5$ mm, $d_0 = 11.5$ mm, $w_0 = 9$ mm, $p_0 = 0$). Similar to Fig. 3, we also plot the boundaries of the gaps of the infinite microstrip. The aforementioned boundaries are delineated by horizontal black-white dotted lines, which permit the identification of edge modes whenever a transmission peak enters the gaps. It is worth noting that if we change only the geometry of the edge cell and do not modify any of the bulk parameters, the edges of the gaps remain unaffected.

Fig. 5a and c show the transmission spectra as a function of the width and length of the central part of the edge cell: w_0 and l_0, respectively. By increasing the width w_0, we can see entering the edge modes from the third band into the second gap ($n = 2$) below at $w_0 = 4$ mm, which reaches the middle of the gap at $w_0 = 12$ mm. The transmission is strongly suppressed by the anti-resonance (marked with the white dashed line), which enters the

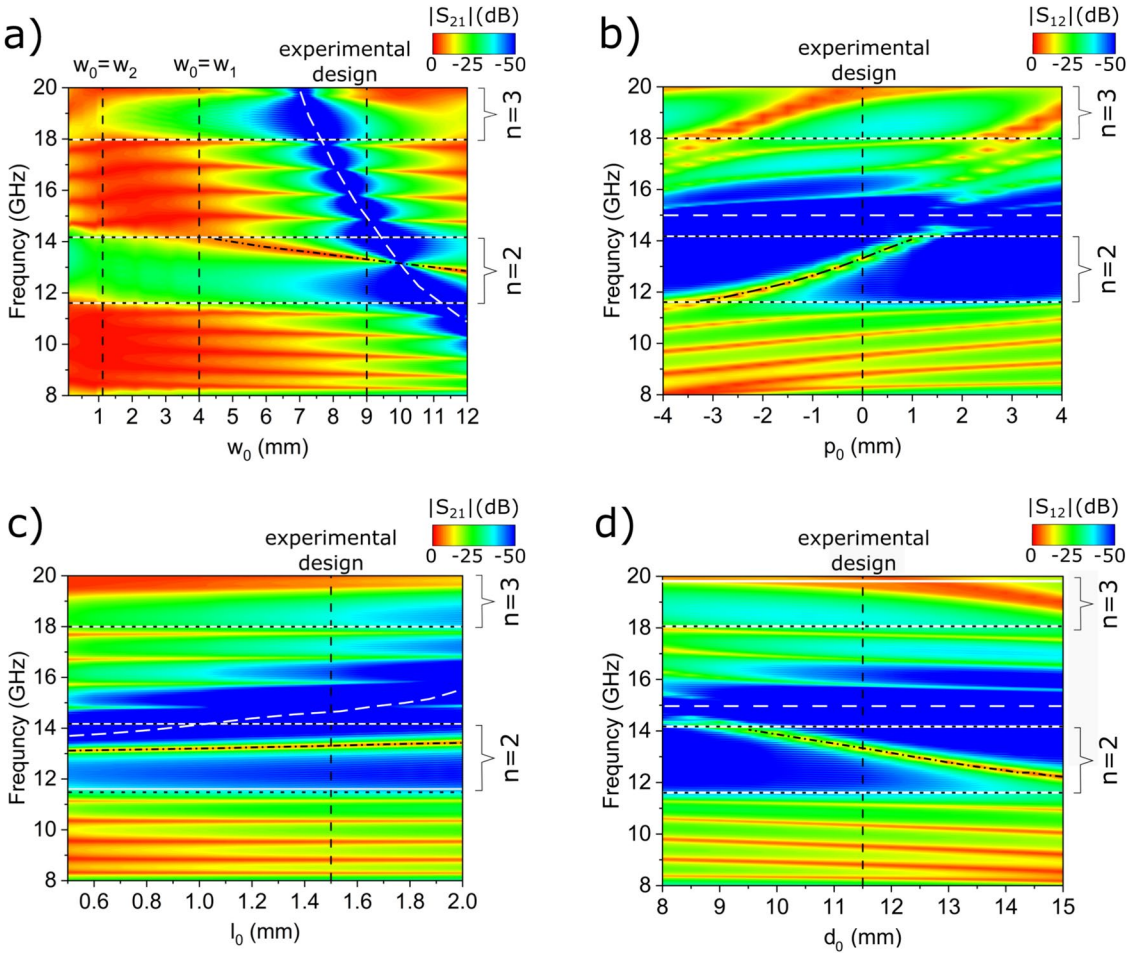

Figure 5. The 2D transmission spectra of the finite periodic microstrip, calculated for different values of the parameters for modified edge cells: (**a**) w_0, (**b**) p_0, (**c**) l_0, (**d**) d_0—see Fig. 1b. We have fixed the values of the bulk parameters to those corresponding to the experimental design, i.e., $l/d = 0.624$; therefore, the edges of the bands (horizontal black dotted lines) are unchanged in this study. For each subplot, we change only one parameter of the edge cells. The rest corresponds to the experimental design (the vertical dashed line indicates the cases where all parameters are the same as for the fabricated structure). We can see that by adjusting the parameters: w_0, p_0, and d_0, one can effectively tune the frequency of the edge modes (black dashed-dotted lines). The strong attenuation in the bands is particularly high for certain values of the parameters: w_0 and l_0, when we observe the sharp minimum in the spectrum—anti-resonance, marked by the white dashed line.

third gap at $w_0 = 7.2$ mm. The frequency of the anti-resonance decreases rapidly with increasing w_0. It deteriorates the transmission in the third band to very low values (below − 50 dB), and also the transmission by edge modes in the second gap ($n = 2$), for $w_0 = 10$ mm. When we set the width to $w_0 = 9$ mm and start detuning l_0 from the experimentally chosen value of 1.5 mm (Fig. 5c). We do not see significant changes in the frequency of the edge mode, only its slight linear increase from 13 GHz to 13.5 GHz with the change of l_0 from 0.5 to 2.0 mm. However, with the changes of l_0 we observe a frequency increase of the anti-resonance. Such a dependence on w_0 and l_0 is understandable since the frequency of the first anti-resonance in the stub transmission is determined by the condition $kw_0/2 = \pi/2$, where k is the wave vector of the interfering wave in the stub—see Supplementary Information S4. This condition holds for a single mode stub, where $w_0/2 \gg l_0$.

Figure 5b,d shows a scenario where we do not change the dimensions of the central part of the edge cell (width w_0 and length l_0), but move it within the edge cells by adjusting p_0 (b), and change the size of the edge cell itself by changing d_0 (d). By adjusting these two parameters we can pull the edge modes across the gap. In particular, the edge modes enter the second gap ($n = 2$) from the bottom at $p_0 = -4$ mm and exit at $p_0 = 1$ mm. In the case of d_0 changes, the frequency of the edge modes enters the gap $d_0 = 9.5$ mm decrease monotonically frequency with increasing d_0. The frequency of the anti-resonance is, as expected, almost unaffected by either p_0 or d_0, but these parameters do influence the impedance matching between the device and ports. From Fig. 5b,d we can deduce that the impedance of the microstrip seen at the ports changes as the length of the section connecting the stub to the microstrip is modified. We can see the edge modes' frequencies increase as this distance shortens (with p_0 increasing or d_0 decreasing).

Resuming, the dependencies illustrated in Fig. 5a–d demonstrate that the frequency of the edge modes in the second gap can be modified by adjusting the shape of edge cells: w_0, p_0, and d_0, whereas the frequency of

the anti-resonance can be controlled by w_0 and l_0. This suggests that the modified edge cell of the microstrip is responsible for both effects, although the underlying physics differs. The independent design of both can be advantageous for various applications since significant transmission suppression is observed around the anti-resonance frequency, exceeding the ± 1 GHz range.

Figure 3d illustrates a doublet peak in transmission through the edge modes, consisting of symmetric and antisymmetric modes (Fig. 4). While the frequency splitting between these modes is minute and barely discernible in the numerical simulations presented in Fig. 3, we utilise the lumped-element method to obtain further insight into the splitting of the edge modes. This model provides the relation between the real system (microstrip) and its simplified but useful description in the form of electrical network—see Supplementary Information S3.

Discussion

We have studied experimentally and numerically the transmission of microwaves through a microstrip of periodically modulated width. We have shown that five repetitions of the unit cell are sufficient to observe the band gaps in the transmission spectrum. We show that this gaps have topological property allowing for the existence of the edge modes.

However, in the undefected microstrip (composed of centrosymmetric unit cells), the edge states cannot exist and the modification of the first and last cell is required to induce them, which was demonstrated experimentally. This effect was explained by relating the topology of the 1D band structure, i.e., the Zak phases of the bands, to the wave impedance of the microstrip (Bloch impedance). The amplitudes of these modes are located at both ends of the microstrip, allowing microwaves to tunnel/leak throughout the entire structure. We can manipulate the edge modes within the desired frequency gap by modifying the geometric parameters of the first and last cell. An alternative method could be to place the microstrip ends on a ferrite layer and tune the frequency of the edge mods using a magnetic field. However, this prospective approach is beyond the scope of this paper and requires new and extensive studies. Nevertheless, the anti-resonance originating from the presence the edge unit cells also impacts the transmission of the microstrip. Thus, using the microstrip for applications such as filtering necessitates careful design of both edge modes and anti-resonance. Fortunately, the geometric parameters of the microstrip's edge cells have a different impact on the frequencies of edge modes and anti-resonance. However, this would require a completely new study, both experimental and numerical.

The edge states appear in the form of a narrow doublet, where the first (second) mode does (does not) flip its phase ϕ while being transmitted through the structure. Therefore, the investigated system can be considered as a passband filter of high selectivity, characterised, in addition, by a significant group delay: $\tau_{\mathrm{gr}} = \frac{1}{2\pi}\frac{d\phi}{df}$. This means that such a filter also plays the role of a delay line. The group delay reaches maxima at frequencies f corresponding to the resonance frequencies of the edge modes. In a relatively narrow range between these resonances, where the transmission is still high, the group delay changes nonmonotonically—see Supplementary Information S5. The rising and falling slopes of the $\tau_{\mathrm{gr}}(f)$ dependence can be used to perform frequency-time mapping[37–39] for the GHz signal simultaneously modulated by few kHz pulses of different frequencies.

Methods

Numerical studies

For the considered periodic microstrips, the transmission spectra S_{21} as well as dispersion diagrams and phase distribution maps were calculated using *CST Microwave Studio*. For the simulation of the dispersion diagrams, the eigenmode calculation with periodic boundary conditions (PBC) in the $z-$ direction was used. The PBC allows modeling an infinite extension of the proposed bulk cell. The "Phase" parameter in PBC is chosen to sweep from 0 to 180 degrees in equal steps, which allows to change the Bloch phase and the associated wave vector from the center to the edge of the 1$^{\mathrm{st}}$ Brillouin zone. The boundary conditions along the $x-$ and $y-$ axes are equivalent to the perfect electrically conducting (PEC) plane. The frequency range starts at 0 Hz and ends at 27 GHz. The Eigenmode Solver has been set to calculate a certain number of the lowest resonant frequencies of the structure since only the fundamental modes are of interest. The Frequency Domain Solver with tetrahedral mesh is used to calculate the S-parameters and the transmission spectra. The following calculation requires the definition of waveguide ports in $z-$ direction through which energy enters and leaves the structure. The open boundary implementation of the solver is the recommended setting. Open boundaries for this type of simulation are implemented as Floquet (Bloch) mode ports and realized in $x-$ and $y-$ planes.

Experimental studies

We used the vector network analyzer (VNA), Agilent N5230A PNA-L, to measure the transmission spectra of the microwaves in the frequency range of 8–20 GHz (see the photo of the experimental setup). The input and output of the microstrip are connected to a vector network analyzer with standard 50 Ω ports to measure the S_{21} spectrum. The unit cell consists of sequentially connected narrow and wide segments. The periodic stripes are etched by photolithography on one side of the Neltec substrate, which is metallized underneath, so that the line consists of five cells and two edge cells. The geometric parameters at the ends of the structure correspond to an input impedance of $Z_0 = 50\,\Omega$. The microwave signal is emitted from one port, transmitted through the structure, and received at another port.

Data availibility

Data supporting this study are openly available from the repository at https://zenodo.org/records/10203785.

Received: 22 December 2023; Accepted: 12 July 2024
Published online: 16 July 2024

References

1. Zak, J. Band center—A conserved quantity in solids. *Phys. Rev. Lett.* **48**, 359–362. https://doi.org/10.1103/PhysRevLett.48.359 (1982).
2. Zak, J. Berry's phase for energy bands in solids. *Phys. Rev. Lett.* **62**, 2747–2750. https://doi.org/10.1103/PhysRevLett.62.2747 (1989).
3. Atala, M. *et al.* Direct measurement of the Zak phase in topological Bloch bands. *Nat. Phys.* **9**, 795–800. https://doi.org/10.1038/nphys2790 (2013).
4. Xiao, M., Zhang, Z. Q. & Chan, C. T. Surface impedance and bulk band geometric phases in one-dimensional systems. *Phys. Rev. X* **4**, 021017. https://doi.org/10.1103/PhysRevLett.48.359 (2014).
5. Yeh, P., Yariv, A. & Hong, C.-S. Electromagnetic propagation in periodic stratified media. I. General theory. *J. Opt. Soc. Am.* **67**, 423–438. https://doi.org/10.1364/JOSA.67.000423 (1977).
6. Vinogradov, A. P. *et al.* Surface state peculiarities in one-dimensional photonic crystal interfaces. *Phys. Rev. B* **74**, 045128. https://doi.org/10.1103/PhysRevB.74.045128 (2006).
7. Kłos, J. Conditions of Tamm and Shockley state existence in chains of resonant cavities in a photonic crystal. *Phys. Rev. B* **76**, 165125. https://doi.org/10.1103/PhysRevB.76.165125 (2007).
8. Malkova, N., Hromada, I., Wang, X., Bryant, G. & Chen, Z. Transition between Tamm-like and Shockley-like surface states in optically induced photonic superlattices. *Phys. Rev. A* **80**, 043806. https://doi.org/10.1103/PhysRevA.80.043806 (2009).
9. Wang, Q., Xiao, M., Liu, H., Zhu, S. & Chan, C. T. Measurement of the Zak phase of photonic bands through the interface states of a metasurface/photonic crystal. *Phys. Rev. B* **93**, 041415. https://doi.org/10.1103/PhysRevB.93.041415 (2016).
10. Yilmaz, D., Yeltik, A. & Kurt, H. Highly controlled Bloch wave propagation in surfaces with broken symmetry. *Opt. Lett.* **43**, 2660. https://doi.org/10.1364/OL.43.002660 (2018).
11. Wang, H.-X., Guo, G.-Y. & Jiang, J.-H. Band topology in classical waves: Wilson-loop approach to topological numbers and fragile topology. *New J. Phys.* **21**, 093029. https://doi.org/10.1088/1367-2630/ab3f71 (2019).
12. Henriques, J. C. G. *et al.* Topological photonic Tamm states and the Su-Schrieffer-Heeger model. *Phys. Rev. A* **101**, 043811. https://doi.org/10.1103/PhysRevA.101.043811 (2020).
13. Xiao, M. *et al.* Geometric phase and band inversion in periodic acoustic systems. *Nat. Phys.* **11**, 240–244. https://doi.org/10.1038/nphys3228 (2015).
14. Yin, J. *et al.* Band transition and topological interface modes in 1D elastic phononic crystals. *Sci. Rep.* **8**, 6806. https://doi.org/10.1038/s41598-018-24952-5 (2018).
15. Li, Z.-W., Fang, X.-S., Liang, B., Li, Y. & Cheng, J.-C. Topological interface states in the low-frequency band gap of one-dimensional phononic crystals. *Phys. Rev. Appl.* **14**, 054028. https://doi.org/10.1103/PhysRevApplied.14.054028 (2020).
16. Wang, L., Cai, W., Bie, M., Zhang, X. & Xu, J. Zak phase and topological plasmonic Tamm states in one-dimensional plasmonic crystals. *Opt. Express* **26**, 28963–28975. https://doi.org/10.1364/OE.26.028963 (2018).
17. Poli, C., Bellec, M., Kuhl, U., Mortessagne, F. & Schomerus, H. Selective enhancement of topologically induced interface states in a dielectric resonator chain. *Nat. Commun.* **6**, 6710. https://doi.org/10.1038/ncomms7710 (2015).
18. Rychły, J. & Kłos, J. W. Spin wave surface states in 1D planar magnonic crystals. *J. Phys. D Appl. Phys.* **50**, 164004. https://doi.org/10.1088/1361-6463/aa5ae1 (2017).
19. Steęślicka, M., Kucharczyk, R. & Glasser, M. L. Surface states in superlattices. *Phys. Rev. B* **42**, 1458–1461. https://doi.org/10.1103/PhysRevB.42.1458 (1990).
20. Kłos, J. & Puszkarski, H. Conditions of coexistence of Tamm and Shockley states in a superlattice with a perturbed surface. *Phys. Rev. B* **68**, 045316. https://doi.org/10.1103/PhysRevB.68.045316 (2003).
21. Marpaung, D., Yao, J. & Capmany, J. Integrated microwave photonics. *Nat. Photonics* **13**, 80–90. https://doi.org/10.1038/s41566-018-0310-5 (2019).
22. Kee, C.-S. *et al.* Essential parameter in the formation of photonic band gaps. *Phys. Rev. E* **59**, 4695–4698. https://doi.org/10.1103/PhysRevE.59.4695 (1999).
23. Guo, J. *et al.* Experimental investigation of interface states in photonic crystal heterostructures. *Phys. Rev. E* **78**, 026607. https://doi.org/10.1103/PhysRevE.78.026607 (2008).
24. Chernovtsev, S. V., Belozorov, D. P. & Tarapov, S. I. Magnetically controllable 1D magnetophotonic crystal in millimetre wavelength band. *J. Phys. D Appl. Phys.* **40**, 295–299. https://doi.org/10.1088/0022-3727/40/2/001 (2007).
25. Zhu, W. *et al.* Zak phase and band inversion in dimerized one-dimensional locally resonant metamaterials. *Phys. Rev. B* **97**, 195307. https://doi.org/10.1103/PhysRevB.97.195307 (2018).
26. Wu, C. H. *et al.* A kind of planar waveguides for cheating the high-speed digital signals into misidentifying the characteristic impedance. *Sci. Rep.* **13**, 14020. https://doi.org/10.1038/s41598-023-41320-0 (2023).
27. Nakata, Y., Ito, Y., Nakamura, Y. & Shindou, R. Topological boundary modes from translational deformations. *Phys. Rev. Lett.* **124**, 073901. https://doi.org/10.1103/PhysRevLett.124.073901 (2020).
28. Mieszczak, S. & Kłos, J. W. Interface modes in planar one-dimensional magnonic crystals. *Sci. Rep.* **12**, 11335. https://doi.org/10.1038/s41598-022-15328-x (2022).
29. Pozar, D. M. *Microwave Engineering* (John Wiley and Sons, 2011).
30. Collin, R. E. *Foundations for Microwave Engineering* (Wiley-IEEE Press, 2001).
31. G.L. Matthaei, L. Y. & Jones, E. *icrowave Filters, Impedance-matching Networks and Coupling Structures* (Artech House Inc., 1980).
32. Berry, M. V. Quantal phase factors accompanying adiabatic changes. *Proc. R. Soc. Lond.* **392**, 45–57. https://doi.org/10.1098/rspa.1984.0023 (1984).
33. Kohn, W. Analytic properties of Bloch waves and Wannier functions. *Phys. Rev.* **115**, 809–821. https://doi.org/10.1103/PhysRev.115.809 (1959).
34. Zak, J. Symmetry criterion for surface states in solids. *Phys. Rev. B* **32**, 2218. https://doi.org/10.1103/PhysRevB.32.2218 (1985).
35. Tsukerman, I. & Markel, V. A. Topological features of Bloch impedance. *Europhys. Lett.* **144**, 16002. https://doi.org/10.1209/0295-5075/acfe93 (2023).
36. Shockley, W. On the surface states associated with a periodic potential. *Phys. Rev.* **56**, 317–323. https://doi.org/10.1103/PhysRev.56.317 (1939).
37. Lyons, W. *et al.* High temperature superconductive wideband compressive receivers. *IEEE Trans. Microw. Theory Tech.* **44**, 1258–1278. https://doi.org/10.1109/22.508231 (1996).
38. Abielmona, S., Gupta, S. & Caloz, C. Compressive receiver using a CRLH-based dispersive delay line for analog signal processing. *IEEE Trans. Microw. Theory Tech.* **57**, 2617–2626. https://doi.org/10.1109/TMTT.2009.2031927 (2009).
39. Kumar, R. & Vinoy, K. J. Large group delay in microstrip circuit using coupled open stubs and collocated ground slots. *IEEE Microw. Wirel. Compon. Lett.* **30**, 553–556. https://doi.org/10.1109/LMWC.2020.2992104 (2020).

Acknowledgements

This work was supported by NCN Poland project no. UMO-2020/39/I/ST3/02413 and the European Union's Horizon 2020 research and innovation programme under the Marie Skłodowska-Curie grant agreement No 644348 (MagIC), and the Polish agency NAWA under the grant No PPN/BUA/2019/1/00114. J.W.K. would like

to acknowledge the support of the Foundation of Alfried Krupp Kolleg Greifswald. The authors would like to thank Andriy E. Serebryannikov for fruitful discussion, are grateful to M. Baranowski and S. Mieszczak for their contributions in the early stages of this work.

Author contributions

S.T. designed the experiments, A.G. and G.K. performed measurements of microwave frequency spectra, A.G. fabricated the microstrip under study. L.I. and S.P. performed the numerical simulations. M.K. and J.W.K. conducted the theoretical analysis. L.I. provided the description of the methods section. All authors contributed to the manuscript.

Competing interests

The authors declare no competing interests.

Additional information

Supplementary Information The online version contains supplementary material available at https://doi.org/10.1038/s41598-024-67610-9.

Correspondence and requests for materials should be addressed to L.I.

Reprints and permissions information is available at www.nature.com/reprints.

Publisher's note Springer Nature remains neutral with regard to jurisdictional claims in published maps and institutional affiliations.